Published in IET Renewable Power Generation
Received on 30th May 2012
Accepted on 15th January 2013
doi: 10.1049/iet-rpg.2012.0361

ISSN 1752-1416

Thyristor-based flexible ac transmission system for controlling the vanadium redox flow battery

Leonardo Javier Ontiveros, Pedro Enrique Mercado

CONICET, Instituto de Energía Eléctrica, Universidad Nacional de San Juan, San Juan, Argentina
E-mail: ontiveros@iee.unsj.edu.ar

Abstract: The vanadium redox flow battery (VRB) is a large stationary energy storage system; which presents high-speed response and overload capacity characteristics. The VRB produces a dc voltage between two terminals; so a power conditioning system composed principally by a dc/ac flexible ac transmission system (FACTS), is required in order to connect the battery to the power system. In this regard, this study proposes a new FACTS compensator for controlling the VRB based on a 12-pulse thyristor converter with commutated capacitors on the ac side. This type of compensator offers a good transient response with low-power converter losses. Simulations of the FACTS compensator employing Matlab/Simulink software validate the proposal and show the good performance of the proposed device.

1 Introduction

Renewable power generation, such as wind and solar power, is emerging as a new energy resource in power systems. According to paper [1], wind power generation grew 22% during the last year. As a result of this, the problems caused by wind generation such as flickers or frequency oscillations will increase. Energy storage systems (ESSs) can be employed in order to mitigate the problems caused by the random variations of the primary energy resource. A promising large stationary advanced ESS for this application is the vanadium redox flow battery (VRB), which presents high-speed response and overload capacity characteristics.

The power conditioning system (PCS) is the interface that allows the effective connection of the VRB to the electric power system [2, 3]. The PCS provides a power electronic interface between the ac power system and the VRB, aiming at achieving two major goals: one is to convert electric power either from dc to ac or from ac to dc, and the other is to charge/discharge efficiently the VRB device. The progress in new technologies of PCS units, so-called flexible ac transmission system (FACTS) controllers, is presently leading the use of advanced energy storage solutions in order to enhance the electrical grid performance, providing enough flexibility to adapt to the specific conditions of the power system [4].

The PCS for VRB applications is based on a distribution static synchronous compensator (DSTATCOM) [2–4]. The DSTATCOM is a fast response, solid-state power compensator that belongs to advanced shunt-connected FACTS devices and provides flexible voltage control (regulation and support) at the point of common coupling (PCC) to the utility system for power quality and stability improvements. It can exchange both active and reactive powers with the power system by varying the amplitude and phase angle of the PCS voltage with respect to the PCC voltage. Fig. 1*a* depicts the typical PCS configuration [2–5]. This system consists mainly of a DSTATCOM, the VRB and the interface between the DSTATCOM and the VRB, represented by a bidirectional dc/dc converter. The DSTATCOM consists mainly of a three-phase voltage source converter (VSC) shunt-connected to the network by means of a coupling transformer with line filter and the corresponding control scheme. Usually, the VSC consists of six insulated gate bipolar transistors (IGBTs) with anti-parallel diodes. The integration of the VRB into the dc bus of the DSTATCOM device requires a rapid and robust bidirectional interface to adapt the range of variation in voltage and current levels between both devices. To this aim, manufacturers propose a two-quadrant dc/dc converter topology according to the VRB unit employed in order to obtain a suitable control performance of the overall system [2–5].

However, the use of the DSTATCOM presents several disadvantages: (i) a dc/dc converter is required between the VRB and the VSC [2–5], (ii) the system complexity increases and the efficiency of the PCS decreases [6–8] and (iii) the high cost of IGBT switches increases the PCS capital cost [9–11]. In this regard, this paper proposes a new FACTS compensator based on a 12-pulse bidirectional thyristor converter for controlling the exchange of active power flow between the VRB and the grid. The thyristor converter operates as a current source on the dc side, therefore the dc/dc converter is avoided (Fig. 1*b*).

This paper is structured as follows: the VRB model is developed in Section 2. Then, the models of the proposed compensator and the corresponding control system are developed in Section 3. Simulation tests are performed in Section 4. Finally, the conclusions are presented in Section 5.

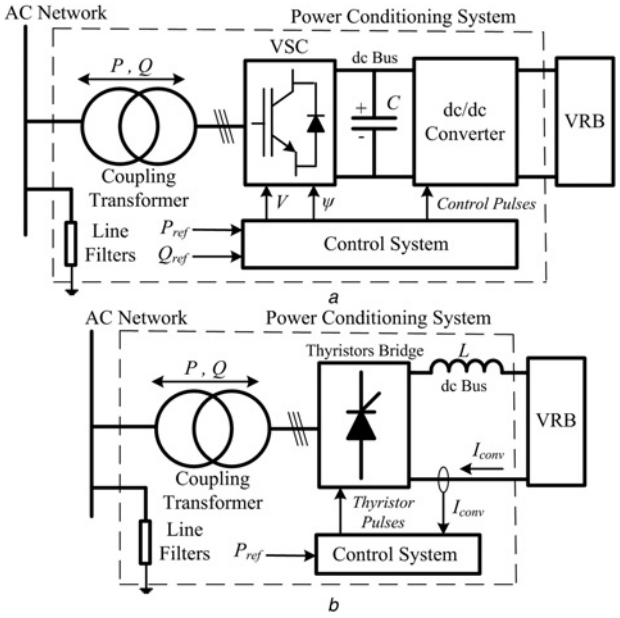

Fig. 1 *PCS unit*
a Typical configuration
b Proposed configuration

2 Vanadium redox flow battery

2.1 General description of the VRB

The VRB is an electrical ESS that converts chemical energy into electrical energy and vice versa [5]. The general scheme of the VRB is shown in Fig. 2*a*. It consists of two electrolyte tanks, containing sulphuric acid electrolyte with active vanadium species in different oxidation states: V_4/V_5 redox couple (catholyte) and V_2/V_3 redox couple (anolyte). These liquids circulate through the cell stack by pumps. The stack consists of many cells, each of which contains two half-cells that are separated by a proton exchange membrane (PEM). In the half-cells, the electrochemical reactions take place on inert carbon felt polymer composite electrodes from which a dc current is used to charge or discharge the battery.

The battery produces a nominal cell potential of ~1.25 V, depending on the concentration of the vanadium. The terminal voltages are achieved by series connection of many cells into a 'stack'. The amount of power available is related to the stack voltage and the current density established through the cell, whereas the energy available depends only on the supply of charged electrolyte to the stack. Hence, the rated power and the energy stored can be readily upgraded by increasing or decreasing the stack and the electrolyte tank, respectively [5].

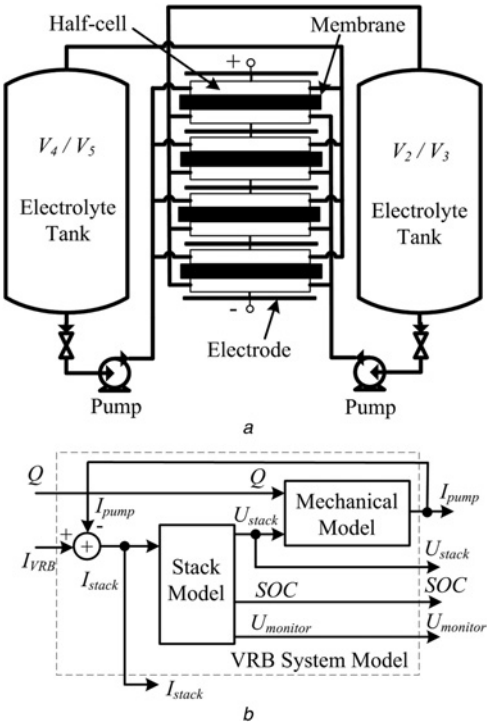

Fig. 2 *Vanadium redox flow battery*
a General scheme
b Mathematical model

2.2 VRB model

The VRB model is composed of two parts: the stack model (electrochemical model), and the mechanical model, as shown in Fig. 2*b* [12]. In the stack model, the terminal VRB current (I_{VRB}) determines the stack current (I_{stack}) and, consequently, the terminal stack voltage (U_{stack}) and the state of charge (SOC) of the electrolyte. In the mechanical model, the external control system sets the flowrate (Q) that produces a pressure drop in the hydraulic system. The energy required to pump the electrolyte is provided by two dc machines. Hence, the pump current consumption (I_{pump}) is subtracted from the terminal current I_{VRB} in order to obtain the stack current I_{stack}.

2.2.1 VRB stack model: The proposed electrochemical model of the VRB calculates two gains in order to obtain the stack voltage U_{stack} and the effective current I_{ef}. These parameters are the voltage and current gains (K_{v}, K_{c}) and they are obtained by solving (1) and (2). Note that K_{c} and K_{v} gains depend on the stack current, the experimental efficiency curves (Fig. 3) [13, 14] and the operating condition (charge or discharge)

$$K_{\mathrm{c,charge}}(I_{\mathrm{stack}}) = \eta_{\mathrm{c}} K_{\mathrm{c,disch}}(I_{\mathrm{stack}}) = \eta_{\mathrm{c}} \frac{(1+\eta_{\mathrm{v}})}{(1+\eta_{\mathrm{e}})} \quad (1)$$

$$K_{\mathrm{v,charge}}(I_{\mathrm{stack}}) = \frac{K_{\mathrm{v,disch}}(I_{\mathrm{stack}})}{\eta_{\mathrm{v}}} = \frac{(1+\eta_{\mathrm{c}})}{(1+\eta_{\mathrm{e}})} \quad (2)$$

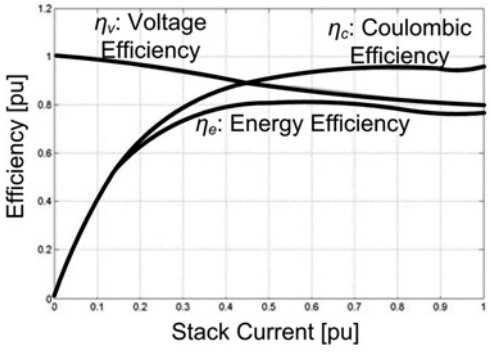

Fig. 3 *Voltage, coulombic and energy efficiencies of the VRB stack*

doi: 10.1049/iet-rpg.2012.0361

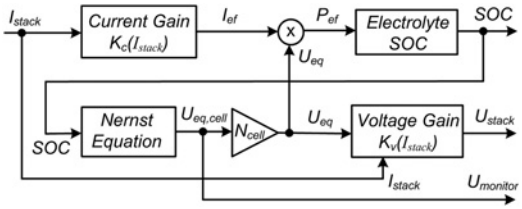

Fig. 4 *Schematic representation of the VRB stack model based on the efficiency curves*

The effective stack current and the terminal stack voltage are obtained with (3) and (4)

$$I_{\text{ef}} = K_{\text{c}}\left(I_{\text{stack}}\right) I_{\text{stack}} \tag{3}$$

$$U_{\text{stack}} = K_{\text{v}}\left(I_{\text{stack}}\right) U_{\text{eq}} \tag{4}$$

The equilibrium voltage (U_{eq}) can be calculated employing the Nernst equation (5) [15–18]

$$U_{\text{eq}} = N_{\text{cell}}\left[U_0 + \frac{2RT}{F}\ln\left(\frac{\text{SOC}}{1-\text{SOC}}\right)\right] \tag{5}$$

where N_{cell} is the number of cells in series connection, U_0 is the internal cell voltage when the SOC is 0.5 pu, R is the gas constant, T is the temperature and F is the Faraday constant. The value of SOC depends on the initial conditions (SOC_0), the storage capacity ($E_{\max}$) and the effective stack power (6) [2, 19]. The schematic representation of the stack model is shown in Fig. 4.

$$\text{SOC} = \text{SOC}_0 + \int \frac{-U_{\text{eq}} I_{\text{ef}}}{E_{\max}}\,\text{d}t \tag{6}$$

2.2.2 Mechanical model: The work presented in [12] develops the mechanical model of the VRB system. This model is composed of an analytical part that models the pipes, bends, valves, tanks and pumps, and a numerical part obtained from a finite element method that describes the more complex stack hydraulic circuit. The mechanical model calculates the total power consumption of the pumps ($P_{2\text{pump}}$) which is caused by the electrolyte flowrate. In addition to the mechanical model, in this paper it is suggested to incorporate the equivalent dc current consumption of the pumps (I_{pump}). Therefore the value of I_{pump} represents the mechanical losses of the VRB system (7).

$$I_{\text{pump}} = \frac{P_{2\text{pumps}}}{U_{\text{stack}}} \tag{7}$$

3 New PCS unit for the VRB

In order to connect the VRB battery to the power system, it is required a dc/ac bidirectional converter that acts as a current source on the dc side. A thyristor-based converter circuit has the potential of charging or discharging the VRB at constant current, as required by the PEM. In this regard, a 12-pulse thyristor converter with commutated capacitors on the ac side (TCCC) is proposed for controlling the active power of the VRB. The TCCC operates as a current source, so its function is to establish the charge or discharge currents (I_{conv}) of the VRB. On the other hand, the voltage at the dc bus (V_{conv}) is determined by the polarisation voltage of the VRB stack. Therefore it is possible to connect the VRB to the TCCC without a dc/dc converter. Fig. 5 shows the proposed PCS unit for the VRB system.

The most important aspects of the proposed PCS are:

- Since a thyristor can only be turned on when there is a positive voltage across it, the converter can only draw an inductive current from the ac network.
- A valve cannot be turned off actively. Instead, the current through one valve has to be brought to zero by turning on another valve (a process known as commutation). The converter has to be operated in such a way that the voltage across the valve that has just turned off remains negative for a sufficiently large time after the commutation.
- The additional voltage provided by the capacitors C_{con} greatly reduces the reactive power consumption of the converter and the risk of commutation failures even in weak ac systems.
- The ac current contains harmonics of order $12n \pm 1$, which are smoothed with tuned filters. In addition, the filters provide the reactive power required by the thyristor converter.

3.1 PCS model

The proposed PCS is composed of two bidirectional Graetz bridges, a coupling transformer with three windings,

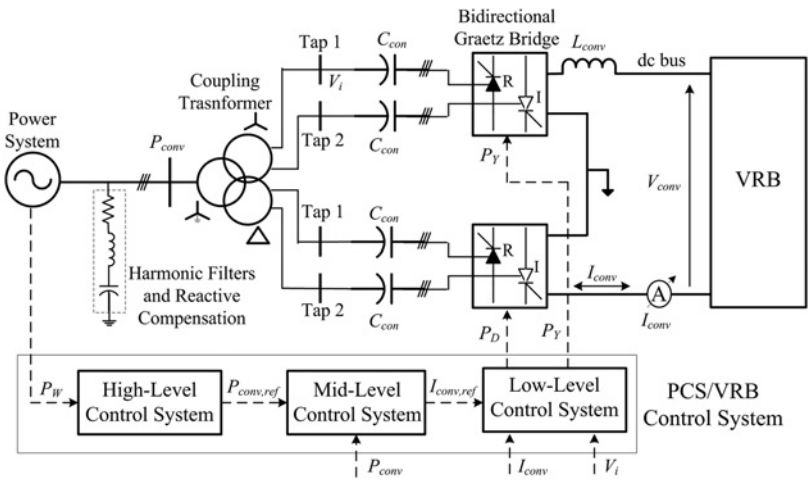

Fig. 5 *Proposed PCS unit*

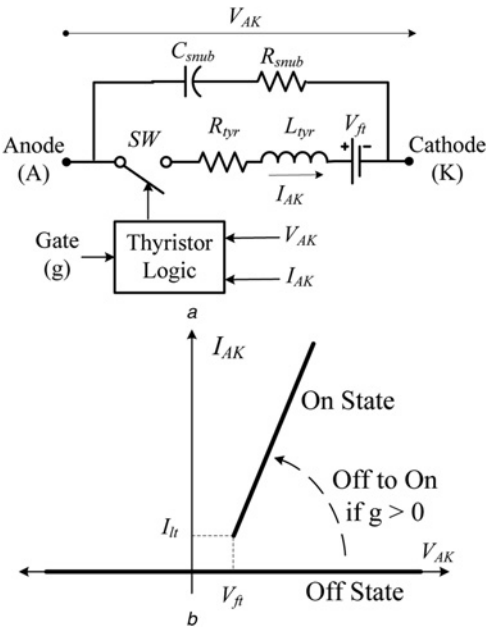

Fig. 6 *Thyristor model and its static VI characteristics*

a Thyristor model
b Static *VI* characteristic of the thyristor

harmonic filters and passive elements (resistances, inductances, capacitors), as shown in Fig. 5. The thyristor is modelled as a resistor R_{tyr}, an inductor L_{tyr} and a dc voltage source representing the forward voltage V_{ft}, connected in series with a switch (Fig. 6*a*). The switch is controlled by a logical signal depending on the voltage V_{AK}, the current I_{AK}, and the gate signal g. The thyristor model also contains a series R_{snub}–C_{snub} snubber circuit, which is connected in parallel with the thyristor device. The static *VI* characteristic of this model is shown in Fig. 6*b*.

3.2 Control system of the PCS

This paper proposes a multi-level control system for the proposed PCS unit; this control system has its own control objectives for each hierarchical control level. Thus a complex control system is divided into several hierarchical levels, which are simpler to design. Owing to each control level is independent of the others and all variables are locally measured, it is possible to adapt advanced control schemes [20]. The proposed multi-level control system is shown in Fig. 7, which is composed of three parts: a low-level control system, a mid-level control system and a high-level control system.

3.2.1 High-level control system: The high-level control system sets the power reference ($P_{conv,ref}$) for the TCCC (Fig. 7). In this case, the goal of the control algorithm is to perform the load levelling of a wind generator. This is accomplished by eliminating the turbulent component of the wind power (P_w). Therefore a first-order filter with a cutoff frequency at 1 cycle/h is employed in order to obtain the diurnal and synoptic component of the wind power (P_{wds}) [21–25]. The difference between P_{wds} and P_w is the compensation power $P_{conv,ref}$ that must be supplied or absorbed by the PCS/VRB unit.

3.2.2 Mid-level control system and low-level control system: Basically, the mid-level control system and the low-level control system operate the TCCC as a controlled current source. Thus, the converter sets a controllable dc current at the VRB terminals, both for charging or discharging. Fig. 7 shows the control algorithm employed. In the mid-level control system, the converter power (P_{conv}) is compared with the compensation power $P_{conv,ref}$; the error signal enters to a proportional-integral (PI) controller in order to obtain the dc reference current ($I_{conv,ref}$). A dead zone block is employed because of the non-linearity of the converter at low current. In the low-level control system,

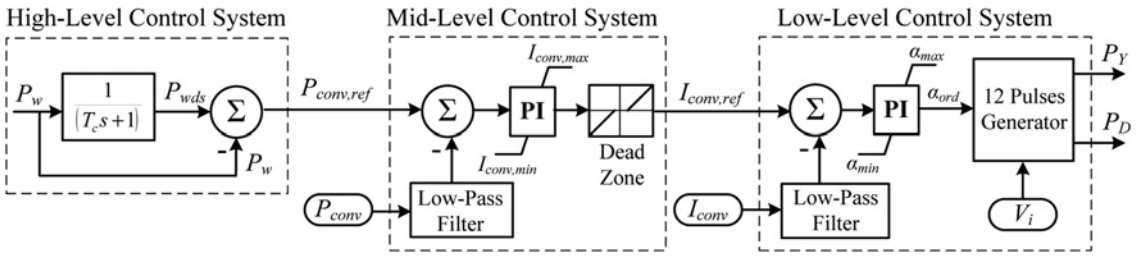

Fig. 7 *Control system of the PCS unit*

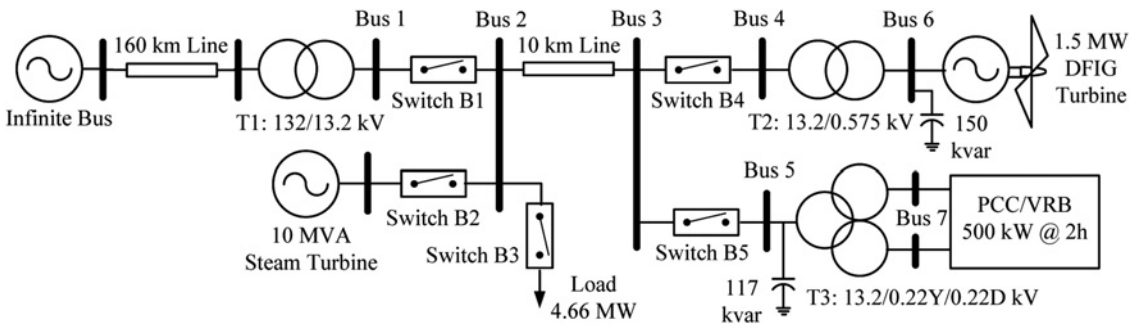

Fig. 8 *Model power system*

doi: 10.1049/iet-rpg.2012.0361

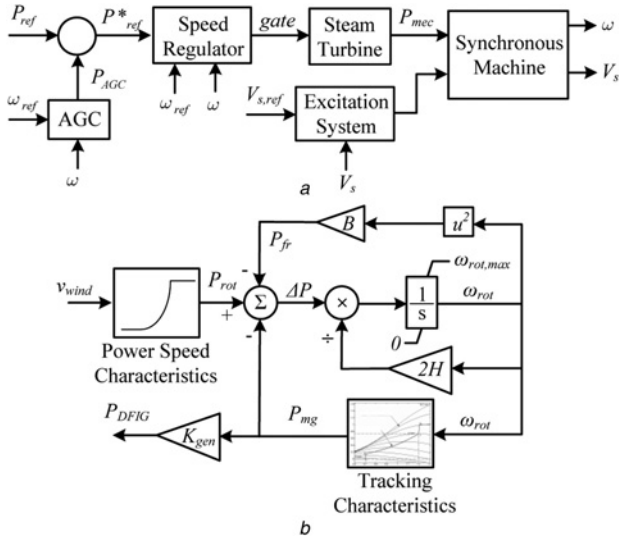

Fig. 9 *Power system modelling*

a Steam turbine model
b DFIG model

the converter current (I_{conv}) is compared with the reference current $I_{conv,ref}$, the error signal enters to a PI controller in order to obtain the firing angle (α_{ord}) for the thyristors. Finally, a 12-pulse generator measures the value of α_{ord}, detects the zero-crossings of the voltage waveforms (V_i) and generates the firing pulses for the TCCC [26, 27]. The mid-level and low-level control systems employ two low-pass filters in order to eliminate the noise signal.

4 Simulation studies

4.1 Model power system

A typical model power system shown in Fig. 8 is used for simulation studies by use of SimPowerSystems® package of the Matlab/Simulink software. This model system is composed of a 132 kV bulk power system (represented as an infinite ac bus) connected to a 13.2 kV network through a 160 km transmission line. The 13.2 kV sub-system is comprised of a 10 MVA steam turbine, a constant load, a 1.5 MW double-fed induction generator (DFIG) wind turbine and a 500 kW PCS/VRB unit. The mathematical models employed in simulations are presented in what follows.

4.1.1 Steam turbine model: The steam turbine model implements a complete tandem-compound steam prime mover, including a speed governing system, an automatic generation control system (AGC), a four-stage steam turbine and a shaft with up to four masses (Fig. 9*a*). The speed governing system consists of a proportional regulator, a speed relay and a servomotor controlling the turbine valve. The AGC consists of a PI regulator, which performs the secondary frequency control. The steam turbine has four expansion stages, each modelled by a first-order transfer function. The first expansion stage represents the steam chest whereas the three other expansion stages represent either reheaters or crossover piping. In this paper, the load variations of the steam turbine are $<4\%$, therefore the boiler pressure is assumed constant during the simulation time [28].

4.1.2 DFIG model: The DFIG model is presented in Fig. 9*b*. This model employs the power speed characteristic of the rotor, which sets the relationship between the wind speed v_{wind} and the mechanical rotor power P_{rot}. The differential mechanical power (ΔP) depends on P_{rot}, the rotor friction losses (P_{fr}) and the generator mechanical power (P_{mg}) obtained from the tracking characteristics. The value of ΔP and the inertia coefficient H determines the instantaneous rotor angular speed (ω_{rot}.). Owing to the generator power losses, a constant gain <1.0 is used for the calculation of the DFIG active power (P_{DFIG}). The estimation of the stator and rotor active power is developed in [29]. The numerical method used for the wind speed calculation is obtained from [29–31].

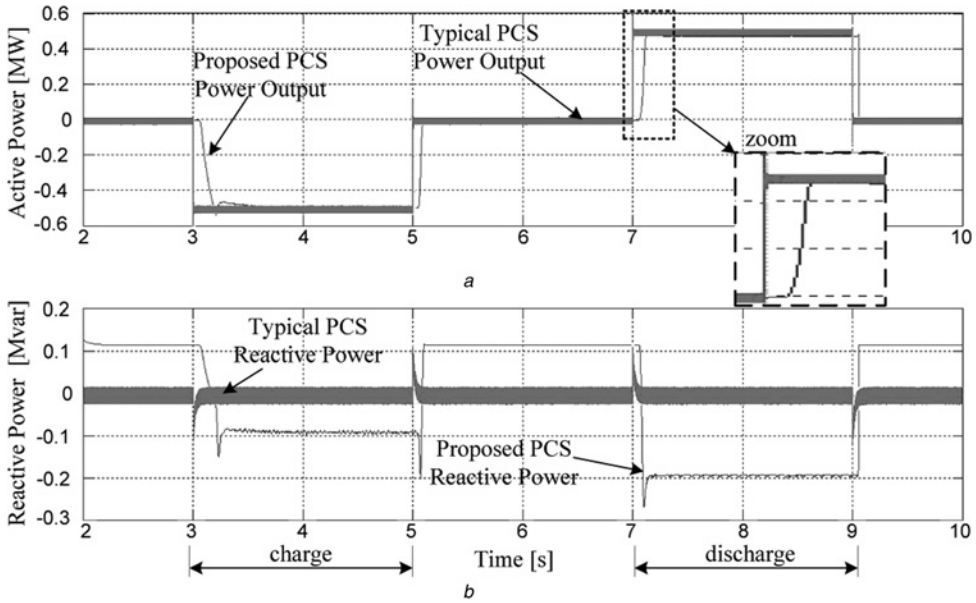

Fig. 10 *Step response of the PCS/VRB unit*

a Active power
b Reactive power

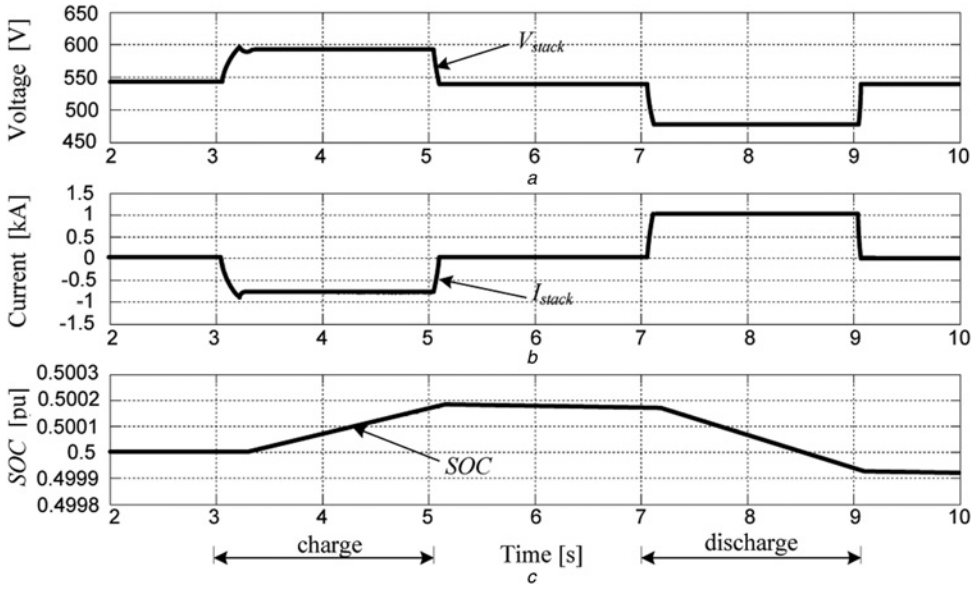

Fig. 11 *Dynamic response of the VRB employing the proposed PCS*

a Stack voltage
b Stack current
c State of charge

4.2 Simulation results

The validation of control algorithms proposed for the PCS/VRB is performed through simple events that impose high demands on dynamic response of the device. In this regard, there are considered two case studies. The first case (Case 1) shows the step response of the PCS/VRB unit. The second case (Case 2) evaluates the dynamic response of the power system when the DFIG turbine operates at variable rotor speed.

4.2.1 Case 1: step response: In this simulation, the step response of the proposed PCS is compared with the corresponding of the typical PCS. The input signal is applied at the reference current $I_{conv,ref}$ (Fig. 7), whereas the output signal is the PCS/VRB power output measured at Bus 5 (Fig. 8). The active and reactive powers are shown in Figs. 10*a* and *b*, respectively. The active power of the proposed PCS follows the reference with a response time of 200 ms approximately, whereas the response time of the typical PCS is <5 ms. Although the proposed PCS has a slower response time than the corresponding of the typical PCS, this feature is not critical for load levelling applications [4, 28]. According to Fig. 10*a*, the step response of the proposed PCS during the rectification

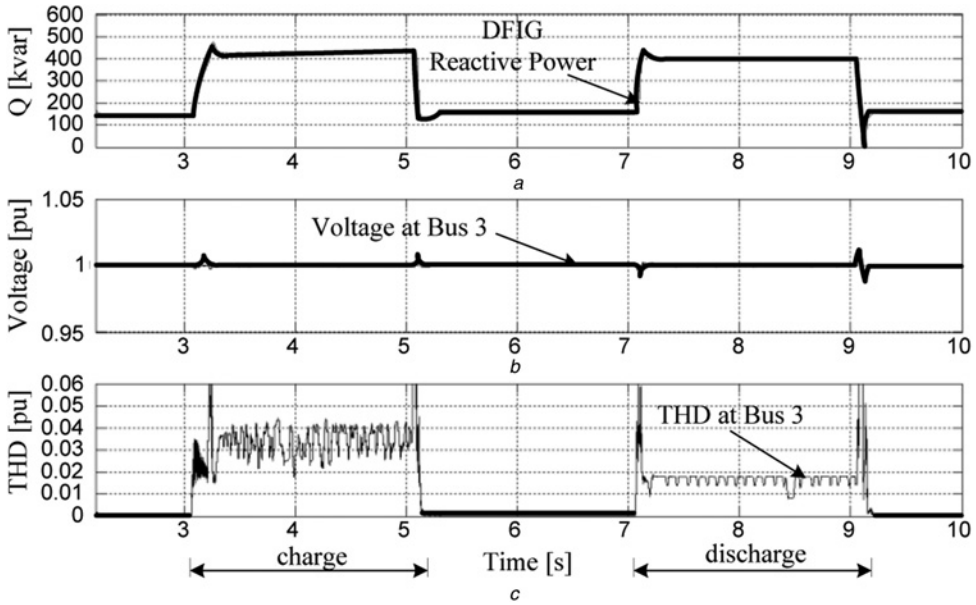

Fig. 12 *Dynamic response of the power system*

a DFIG reactive power
b Voltage at Bus 3
c THD at Bus 3

doi: 10.1049/iet-rpg.2012.0361

(charging) is similar to the performance of a second-order low-pass filter and during the inversion (discharging), the step response is similar to the performance of a first-order low-pass filter.

Regarding to the reactive power consumption, Fig. 10*b* shows that the VAR consumption of the proposed PCS varies in accordance with the dc converter current (I_{conv}) and the VRB polarisation voltage, meanwhile the reactive power output of the typical PCS not varies significantly. This drawback can be mitigated employing reactive power compensation, provided by capacitor banks or by the DFIG turbine.

Fig. 11 shows the dynamic response of the VRB employing the proposed PCS. Fig. 11*a* shows that the stack voltage increases during the charge cycle, and decreases during the discharge cycle. The stack current shown in Fig. 11*b* has the values of -800 A and 1 kA during the charge and discharge cycle, respectively. This difference occurs because of the lower the stack voltage is, the higher the stack current is, in order to obtain the same converter power. Fig. 11*c* shows the electrolyte SOC, which increases during the charge and decreases during the discharge. In this test, the energy transferred to the VRB is equal to the energy released from the VRB in a charge–discharge cycle; however, the final SOC_f is lower than the initial SOC_i. This difference occurs because of the power converter losses, the electrochemical losses and the pump power consumption of the VRB. In this regard, the discharge of the VRB can be avoided by subtracting to the current reference, the estimation of the equivalent dc current losses [26].

The most important aspects of the proposed PCS/VRB unit are:

- The dc-bus voltage V_{conv} varies in accordance with the VRB stack voltage; this voltage depends on the electrolyte SOC and the magnitude and direction of the current I_{conv}. The minimum value of V_{conv} occurs at minimum SOC and maximum discharge current ($-I_{conv}$). The maximum value of V_{conv} occurs at maximum SOC and maximum charge current (I_{conv}).
- The higher the converter current, the higher is the reactive power consumption, especially during the inversion process (discharging).
- The reactive power consumption depends on the secondary winding voltage of the coupling transformer. The higher the secondary voltage, the higher is the converter current; but the reactive power consumption increases. Therefore it is necessary to adopt the minimum value of secondary voltage that meets the requirement of maximum converter current ($I_{conv,max}$). In this regard, because of the stack polarisation voltage increases during the charge and decreases during the discharge, there are two optimal values of secondary winding voltage. To solve this problem, the coupling transformer employs two fixed taps (Taps 1 and 2). Tap 1 is set at minimum voltage required for rectification and Tap 2 is set at minimum voltage required for inversion. Then, Taps 1 and 2 are connected to the rectifier and inverter bridges, respectively (Fig. 5).

The dynamic response of the power system is illustrated in Fig. 12. Fig. 12*b* shows that the DFIG turbine is capable of

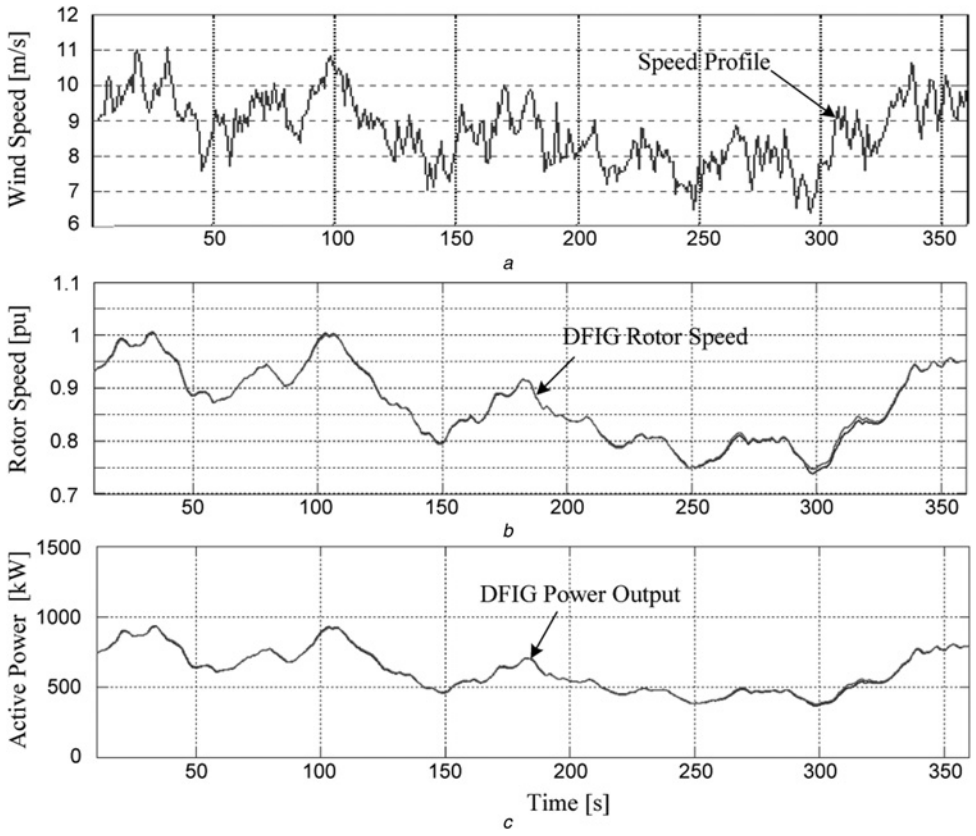

Fig. 13 *Wind speed simulation*

a Wind speed profile
b DFIG rotor speed
c DFIG power output

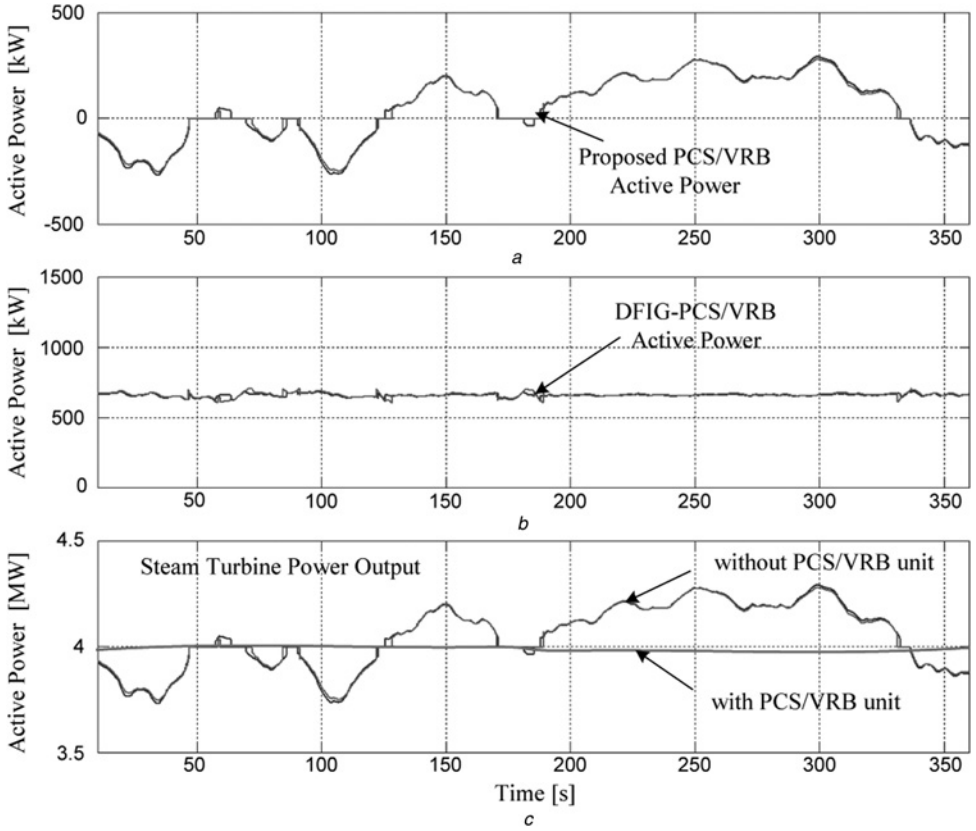

Fig. 14 *Dynamic response of the power system*

a Active power output of the proposed PCS/VRB unit
b DFIG-PCS/VRB active power
c Active power output of the steam turbine

controlling the voltage at Bus 3. The reactive power consumption of the proposed PCS is compensated with the reactive power flow of the DFIG turbine (Fig. 12*a*). On the other hand, Fig. 12*c* illustrates the total harmonic distortion (THD) at Bus 5. The simulation shows that the THD value is $< 5\%$ both for charge and discharge cycles.

This test shows that the proposed PCS provides an acceptable dynamic response both for charging or discharging cycles producing a low level of THD. The reactive power fluctuations generated by the TCCC are compensated by the DFIG generator. In addition, the use of the TCCC instead of the DSTATCOM provides the following advantages: (i) for the same rated power, the capital cost of a TCCC is ~20–30% of the capital cost of a DSTATCOM [9–11], (ii) for power ratings above 1 MW, the TCCC provides a higher efficiency than the DSTATCOM (from 85 to 99%) [6–11, 32, 33] and (iii) the proposed PCS is less complex than the typical PCS because of the dc/dc converter can be avoided.

4.2.2 Case 2: dynamic response by wind speed variations: This test simulates the wind speed employing the numerical procedure developed in [29, 31]. Fig. 13*a* illustrates the wind speed, which is composed of two components: a short-term component (turbulence) plus a long-term component (diurnal and synoptic variations). The dynamic response of the DFIG turbine is shown in Figs. 13*b* and *c*. In this case, the turbine operates at variable rotor speed (Fig. 13*b*). Therefore the rotor acts as an ESS by smoothing 40% of the turbulence (Fig. 13*c*).

The simulation is performed considering the worst case: the 13.2 kV power system in island operation (Switch B_1 of Fig. 8 in 'off'). Therefore the steam turbine controls the frequency of the system. The load is set constant, but the wind power varies according to Fig. 13*c*, thus the steam turbine controls the system frequency by compensating the DFIG-PCS/VRB active power flow. The power output of the proposed PCS is illustrated in Fig. 14*a*; the positive values correspond to discharge cycles. Figs. 14*b* and *c* show the DFIG-PCS/VRB power flow and the active power output of the steam turbine; both of them are smoothed by the proposed PCS/VRB unit.

This test shows that the proposed PCS/VRB unit enhances the dynamic response of the power system. It is important to note that the DFIG turbine and the PCS/VRB unit complement each other; the fluctuations of the wind power generation are smoothed by the PCS/VRB unit, whereas the reactive power fluctuations generated by the TCCC are compensated by the DFIG generator.

5 Conclusions

This paper proposes a new PCS unit for the VRB; the PCS employs a TCCC compensator instead of the typical configuration with the DSTATCOM device. The TCCC device consists of a 12-pulse TCCC. The thyristor converter operates as a current source, avoiding the use of the dc/dc converter needed by the typical PCS configuration. In order to control the PCS, a three-level control system was developed. The external control system sets the power that exchanges the VRB with the power system. The aim of this

doi: 10.1049/iet-rpg.2012.0361

power flow is to smooth the power generated by a DFIG turbine. The medium control level sets the direct current at the battery terminals, and the internal control level calculates the firing angles and generates the thyristors firing pulses. The model aspects of the control system and the PCS unit are also presented in this paper.

From the results obtained, it can be concluded that the proposed PCS compensator works satisfactorily, by controlling the power flow exchanged between the VRB and the power system. In this regard, the PCS/VRB unit compensates the wind power variations generated by the DFIG turbine, and enhances the dynamic response of the power system. For the reactive power control, it is shown that the DFIG is able to compensate the reactive power consumption of the TCCC, and also to provide a unitary power factor at the PCC.

6 Acknowledgments

This work was partially financed by the Consejo Nacional de Investigaciones Científicas y Técnicas (CONICET), Argentina.

7 References

1 www.wwindea.org. World Wind Energy Association website, accessed November 2012. Available from: http://www.wwindea.org/webimages/Half-year_report_2012.pdf
2 Chen, Z., Ding, M., Su, J.: 'Modeling and control for large capacity battery energy storage system'. Proc. Int. Conf. on Electric Utility Deregulation and Restructuring and Power Technologies (DRPT), Weihai, China, July 2011, pp. 1429–1436
3 Taylor, G., Smith, C., Irving, M.: 'Flow batteries for enhancing wind power integration', *IEEE Trans. Power Syst.*, 2012, **27**, (3), pp. 1690–1697
4 Molina, M., Suvire, G., Ontiveros, L., Mercado, P.: 'Emerging energy storage technologies in utility power systems: a technical insight', in: '*Energy storage*' Rosen, (Ed.) (Nova Science Publishers Press, 2011, 1st edn.), pp. 235–312
5 www.pdenergy.com. Prudent Energy website, accessed November 2012. Available at http://www.pdenergy.com/vrb-energy-storage-systems.php
6 Klumpner, C., Rashed, M., Patel, C., *et al.*: 'Achieving the desired transformer leakage inductance necessary in DC-DC converters for energy storage applications'. Proc. Int. Conf. on Power Electronics, Machines and Drives (IET/PEMD), Bristol, UK, March 2012, pp. 101–106
7 Du, Y., Lukic, S., Jacobson, B., *et al.*: 'Modulation technique to reverse power flow for the isolated series resonant DC-DC converter with clamped capacitor voltage', *IEEE Trans. Ind. Electron.*, 2012, **59**, (12), pp. 4617–4628
8 Ahmadi, M., Shenai, K.: 'New, efficient, low-stress buck/boost bidirectional DC-DC converter'. Proc. Int. Conf. on EnergyTech (IEEE/EnergyTech), Cleveland, USA, May 2012, pp. 1–6
9 Tolbert, L., King, T., Ozpineci, B., *et al.*: 'Power electronics for distributed energy systems and transmission and distribution applications' Technical Report, Engineering Science and Technology Division, The University of Tennessee-Knoxville, 2005
10 www.siemens.com. Siemens Global website, accessed November 2012. Available at http://www.energy.siemens.com/hq/en/power-transmission/facts/
11 www.abb.com. The ABB Group website, accessed November 2012. Available at http://www.abb.com/industries/es/9AAC30100023.aspx?country=AR
12 Blanc, C., Ruffer, A.: 'Multiphysics and energetic modeling of a vanadium redox flow battery'. Proc. Int. Conf. on Sustainable Energy Technologies (ICSET), Singapore, October 2008, pp. 759–764
13 Wang, G.: 'Minimising output power fluctuation of large photovoltaic plant using vanadium redox battery storage'. Proc. Int. Conf. on Power Electronics, Machines and Drives (IET/PEMD), Bristol, UK, March 2012, pp. 1–6
14 Wang, G.: 'PV power plant using hybrid energy storage system with improved efficiency'. Proc. Int. Conf. on Power Electronics for Distributed Generation Systems (IEEE/PEDG), Aalborg, Denmark, June 2012, pp. 808–813
15 Chahwan, J., Abbey, C., Joos, G.: 'VRB modelling for the study of output terminal voltages, internal losses and performance'. Proc. Int. Conf. on Electric Power Conference (EPC), Montreal, Canada, October 2007, pp. 387–392
16 Skyllas-Kazacos, M., Menictas, C.: 'The vanadium redox battery for emergency back-up applications'. Proc. Int. Conf. on Telecommunications Energy Conf. (INTELEC), Melbourne, Australia, October 1997, pp. 463–471
17 Mousa, A.: 'Chemical and electrochemical studies of V(III) and V(II) solutions in sulfuric acid solution for vanadium battery applications'. *PhD thesis*, University of South Wales (UNSW), Australia, 2003
18 Tsuda, I., Kurokawa, K., Nozaki, K.: 'Development of intermittent redox flow battery for PV system'. Proc. Int. Conf. on World Conf. Photovoltaic Energy Conversion (WCPEC), Honolulu, Hawaii, December 1994, pp. 946–949
19 Wang, W.: 'Grid-connected wind farm power control using VRB-based energy storage system'. Proc. Int. Conf. on Energy Conversion Congress and Exposition (IEEE/ECCE), Delft, Netherlands, August 2010, pp. 3772–3777
20 Suvire, G., Mercado, P.: 'DSTATCOM with flywheel energy storage system for wind energy applications: control design and simulation', *Electr. Power Syst. Res.*, 2010, **80**, (3), pp. 345–353
21 Xu, Z., Ehsani, M.: 'Reconstruction of effective wind speed for fixed-speed wind turbines based on frequency data fusion'. Proc. Int. Conf. on 23rd Electrical and Computer Engineering (CCECE), Alberta, Canada, May 2010, pp. 1–9
22 Veszpremi, K., Schmidt, I.: 'Flywheel energy storage drive for wind turbines'. Proc. Int. Conf. on Power Electronics and Drive Systems (PEDS), Bangkok, Thailand, November 2007, pp. 916–923
23 Söder, L., Ackermann, T.: 'Wind power in power systems: an introduction', in Ackermann, T. (Ed.): '*Wind power and power system*' (John Wiley and Sons Press, 2005, 1st edn.), pp. 33–39
24 Nichita, C., Luca, D., Dakyo, B., Ceanga, E.: 'Large band simulation of the wind speed for real time wind turbine simulators', *IEEE Trans. Energy Convers.*, 2002, **17**, (4), pp. 523–529
25 Van der Hoven, I.: 'Power spectrum of horizontal wind speed in the frequency range from 0.0007 to 900 cycles per hour', *J. Meteorol.*, 1956, **14**, (2), pp. 160–164
26 Sood, V.: 'HVDC transmission', in Rashid, M. (Ed.): '*Power electronic handbook*' (Academic Press, 2001, 1st edn.), pp. 575–596
27 www.mathworks.com. Matlab and Simulink website, accessed November 2012. Available at http://www.mathworks.com/help/physmod/powersys/ref/synchronized12pulsegenerator.html
28 Silvestri, G.: 'Steam turbines', in Elliot, T. (Ed.): 'Standard handbook of powerplant engineering' (McGraw-Hill Press, 1989, 1st edn.), pp. 2.25–2.61
29 Ontiveros, L., Mercado, P., Suvire, G.: 'A new model of the double-fed induction generator wind turbine'. Proc. Int. Conf. on IEEE/PES Transmission and Distribution, Sao Paulo, Brazil, November 2010 pp. 1–7
30 Ontiveros, L., Mercado, P.: 'Modeling of variable-speed wind farms for power systems dynamic studies'. Proc. Int. Conf. on XIV ERIAC, Ciudad del Este, Paraguay, May 2011
31 Burton, T., Sharpe, D., Jenkins, N., Bossanyi, E.: 'The wind resource', in Burton, T. (Ed.): 'Wind energy handbook' (John Wiley and Sons Press, 2005, 1st edn.), pp. 11–38
32 Jenkins, N.: 'Application of power electronics to the distribution system', in Song, Y., Johns, A. (Eds.): 'Flexible AC transmission systems (FACTS)' (TJ International Press, 1999, 1st edn.), pp 546–574
33 Hingorani, N., Gyugyi, L.: 'Static shunt compensators: SVC and STATCOM', in Hingorani, N. (Ed.): 'Understanding FACTS – concepts and technology of flexible AC transmission systems' (IEEE Press, 2000, 1st edn.), pp 135–207